
Proceedings Paper:
Merino Perez, J.L., Hodzic, A., Merson, E. et al. (1 more author) (2015) Induced thermo-mechanical damage in the drilling of thermoplastic-toughened CFRP composites. In: Proceedings of;. 20th International Conference on Composite Materials, 19-24th July 2015, Copenhagen, Denmark. .

INDUCED THERMO-MECHANICAL DAMAGE IN THE DRILLING OF THERMOPLASTIC-TOUGHENED CFRP COMPOSITES

J.L. Merino-Pérez[1], R. Royer[2], S. Ayvar-Soberanis[3], E. Merson[2] and A. Hodzic[4]

[1] Industrial Doctorate Centre in Machining Science, Department of Mechanical Engineering, The University of Sheffield, Sir Frederick Mappin Building, Mappin Street, Sheffield, S1 3JD, UK. Contact: j.merino@sheffield.ac.uk

[2] Sandvik Coromant, Sandvik AB. Advanced Manufacturing Park, Unit 8, Morse Way, Waverley, Sheffield, S60 5BJ, UK. Contacts: raphael.royer@sandvik.com, eleanor.merson@sandvik.com

[3] Advanced Manufacturing Research Centre with Boeing, The University of Sheffield, Advanced Manufacturing Park, Wallis Way, Catcliffe, Rotherham, S60 5TZ, UK. Contact: s.ayvar@amrc.co.uk

[4] Composite Systems Innovation Centre, Department of Mechanical Engineering, The University of Sheffield, Sir Frederick Mappin Building, Mappin Street, Sheffield, S1 3JD, UK. Contact: a.hodzic@sheffield.ac.uk

Keywords: Drilling of composites, CFRP, Thermosetting resin, Nanoindentation, Damage tolerance

ABSTRACT

This investigation focused on the assessment of the induced thermal and mechanical damage in the drilling of carbon fibre reinforced polymer (CFRP) composites in the 50-200m/min cutting speed range. 3D surface measurement techniques were used to assess the induced mechanical damage by studying the drilled surface and successfully related selected surface parameters to specific types of defects (splintering, fibre pull-out and crater). The workpiece constituents, especially the type of reinforcement, showed significant impact on the extent of the induced mechanical damage. The nanoindentation technique studied the induced thermal damage by measuring the bulk properties of the resin phase from the hole edge up to 1 mm away from the borehole. The type of resin, degree of cross-linking and the ageing temperature exhibited strong influence on different ageing stages studied in this work.

1 INTRODUCTION

The utilisation of fibre reinforced polymer (FRP) composites in the automotive and aerospace industry, especially those reinforced with carbon fibres (CFRP), has been dramatically increased for the past few decades due to their high specific mechanical properties. These properties allowed for lightweight transport technologies, which ultimately resulted in lower fuel consumption and reduced the environmental impact [1, 2]. Composites for high in-service temperature applications feature epoxy matrices (thermosetting resins) having a significant cross-linking degree, thus exhibiting improved thermal and mechanical properties [3, 4]. However, highly cross-linked resins also exhibit low impact resistance and fracture toughness and need to be modified with high performance thermoplastic polymers or rubber blends in order to enhance their damage tolerance [5-7]. The addition of toughening elements to thermosetting resins could also modify the morphology and phase distribution of the system, depending on the nature of the toughening agent, the cure cycle and the toughening degree [8-15].

Early work by Kim et al. studied multi-phase toughened epoxies modified with carboxyl-terminated butadiene-acrylonitrile (CTBN) and poly(ether sulphone) (PES), which resulted in binary and ternary blends. They discovered that in the binary blends phase separation occurred during the curing stage, whereas in the ternary blends this occurred in two stages: macrophase separation occurred during the mixing stage followed by microphase separation in the curing stage. Morphology and mechanical properties of ternary blends showed to be more sensitive to the composition, showing

different dominant phases depending on the toughening agent content and a significant variation in the elastic modulus and yield stress.

Gan et al. investigated the viscoelastic effects on the phase separation in epoxy systems (diglycidyl ether of bisphenol A/methyltetrahydrophthalic anhydride, DGBA–MTHPA) modified with thermoplastics (polyetherimide, PEI) having different quantities of curing accelerator, by applying time-resolved light scattering (TRLS) and scanning electron microscopy (SEM) techniques [9]. The results indicated that the phase separation occurred according to the spinodal decomposition (SD) mechanism earlier described by Tanaka [16, 17], and determined that the phase separation and morphologies obtained could be influenced by the kinetic factor and the viscoelastic effects resulting from the different cross-linking degree between the constituents in the studied blends.

Russell and Chartoff studied the effects of curing conditions on the morphology in two-phase DGBA-piperidine-CTBN blends using SEM, dynamic mechanical analysis (DMA) and atomic force microscopy (AFM) [10]. Data showed a direct correlation between rubber particle modulus and the constraint level of the epoxy matrix on the rubber particles, and an inverse correlation with the curing temperature, whereas the volume fraction of the rubber phase was found to reach its maximum at the highest curing temperature. Fracture toughness of the blend resulted in higher rubber volume fraction, however the lowest values of fracture toughness were obtained when the rubber particle modulus was in the high range. This may indicate that the rubber phase must be relatively soft enough in order to enhance the toughness of the blend.

The work conducted by Zhang et al. studied the effect of the curing rate and dwell on the phase separation and Mode I delamination fracture toughness of a thermoplastic-toughened epoxy and a commercial thermoplastic-toughened CFRP composite system [11]. The authors applied real-time Fourier transform infrared spectroscopy, optical and SEM techniques, and combined two different curing rates (1.5 and 10°C/min) with 30 min intermediate curing dwell. The results showed that phase separation increased with the curing rate, and the curing dwell favoured more spherical phases. Mode I delamination fracture toughness investigation of a commercial thermoplastic-toughened CFRP system revealed that rapid curing rates increased Mode I delamination fracture toughness compared to slow curing rates.

Jyotishkumar et al. assessed the impact of curing temperature on the cure kinetics and phase morphology in acrylonitrile butadiene styrene (ABS)-toughened DGEBA-DDS epoxy system by applying rheometry, small-angle light scattering (SALLS), AFM and optical microscopy (OM) techniques. They observed that the curing temperature had significant impact on phase separation. 180°C cure temperature yielded co-continuous phase morphology, whereas inverted type phase morphologies were developed at 150°C and 165°C.

Investigations conducted by Moosburger-Will et al. [13], Rico et al. [14] and Mathew et al. [15] studied the effects of thermoplastic toughеners on the phase separation and morphology of epoxy systems by applying scanning probe microscopy (SPM), SEM, energy-dispersive X-ray spectroscopy (EDX), thermal and mechanical analysis (DMA, TGA) techniques. Moosburger-Will et al. observed two-phase morphology, with rounded particles of epoxy inside the polyetherimide (PEI)-rich phase and PEI particulate precipitation inside the epoxy-rich phase, whereas ribbon-like PEI regions developed small globular structures having sizes ranging from 50 to 500 nm. Rico et al. reported that thermoplastic (polystyrene, PS) content had a significant influence on the phase morphology and three different morphologies developed: sea-island morphology (PS particles dispersed in an epoxy-rich matrix) for low PS proportions, nodular morphology (inverse, epoxy particles in a PS-rich matrix) for high PS proportions and a dual phase morphology combining the previously mentioned morphologies at low-mid PS compositions. Mathew et al. found that rubber domain size and the fracture toughness increased with the increasing epoxidized natural rubber (ENR) proportion, due to coalescence. The fracture toughness enhancing mechanism consisted in the ENR droplets acting as stress concentrators, thus inducing plastic deformation in the surrounding matrix and absorbing a considerable quantity of the exerted stress.

A number of authors also investigated the ageing of toughened multi-phase epoxy resins [13, 18-20]. Early studies by Jong and Yu investigated the effect of PES on the physical ageing (under the glass transition temperature, T_g) of epoxies (DGEBA-DDS) [18]. They observed that at mid-low ageing temperatures the blend showed two enthalpy relaxation processes, where the one that occurred

at the highest temperature corresponded to the epoxy, the lowest one corresponded to the PES. At high ageing temperatures, a single enthalpy relaxation process was observed, in which the relaxation process due to the physical ageing was similar to that of the pure epoxy. On the other hand, the enthalpy relaxation process of PES in the epoxy matrix was similar to that of the pure PES at all studied temperatures.

Lee and McKeena assessed the creep and stress relaxation of a two-phase CTBN-toughened epoxy after ageing the samples between the respective glass transition temperatures of the rubber and the epoxy. The results reported that the stress relaxation curves did not superimpose, however the creep curves superimposed for all ageing times. According to the authors, these results presented an anomalous behaviour for which they considered a number of reasons [19].

Leon Yu and Chen conducted a study to assess the impact of molecular weight of the toughening agent on the ageing behaviour of epoxy systems by preparing three DGBA-DDS-PES blends having different PES molecular weights. The results suggested that a carefully selected ageing temperature would promote phase separations in DGEBA-DDS-PES blends having high molecular weight PES [20]. A more recent study conducted by Moosburger-Will et al. found that the surface elastic modulus of the epoxy regions in the aged samples increased around 12% respect to the non-aged samples, whereas the PEI regions remained unaffected in both cases [13].

The temperatures developed in the drilling of CFRP are often above T_g of the polymer matrix of the composite [21, 22]. Polymer matrices exposed to these ranges of temperatures during short times exhibited thermal ageing in the form of residual cross-linking (or post-curing) and further degradation, depending on the ageing times and temperatures [23], which affected the mechanical performance of the composite [24].

The work presented in this study applied nanomechanical and 3D surface measurement techniques, to assess the thermo-mechanical damage around the borehole in the drilling of three considered CFRP composite systems featuring different thermoplastic-toughened epoxy matrices and carbon fibre reinforcements.

2 MATERIALS AND METHODS

2.1 Composite preparation

The CFRP panels used in this study were manufactured at the Composite Centre of the Advanced Manufacturing Research Centre with Boeing, The University of Sheffield. These CFRP panels were made from prepregs plies having a 55% fibre volume fraction (V_f) supplied by Cytec Engineered Materials following the vacuum bag moulding method. 40 plies were laid-up ($[(0,90)_3/(\pm45)]_{5s}$) to an approximate thickness of 10 mm, following an autoclave curing cycle according to the specifications supplied by the manufacturer to develop optimal mechanical properties and maximum T_g. After their respective curing cycles, the plates were cut down to 150x150 mm using water-jet cutting.

This study considered three composite systems combining two thermosetting resins, MTM44-1 and MTM28B, and two carbon fibre fabrics, CF0300 and CF2216:

- MTM44-1 CF0300,
- MTM44-1 CF2216, and
- MTM28B CF0300.

MTM44-1 is a high performance thermoplastic-toughened phenol-formaldehyde (PF)-based resin having T_g around 190˚C, and MTM28B is a toughened DGEBA-based epoxy resin with T_g of approximately 100˚C. CF0300 is a high strength (HS) woven carbon fibre (CF) fabric featuring 2/2 twill and 3,000 filaments per tow, whereas CF2216 is a high modulus (HM) 2/2 twill woven CF fabric having 6,000 filaments per tow. Both CF fabrics have a density of 199 g/cm^3.

2.2 Drilling tool

The drilling tool utilised was a ϕ6.35mm two flute double angle uncoated tungsten carbide-10% cobalt (WC-Co) supplied by Sandvik Coromant. Full details on the tool geometry is available in our previous work [22]. Each cutting condition used a brand new tool in order to avoid any effect derived from the accumulated tool wear. The CNC machine considered to perform the drilling operations was a three axis Mori DMU 60monoBLOCK. All the drilling operations in this investigation were performed in dry conditions.

2.3 Mechanical damage around the hole edge in the drilling of CFRP composites

This work assessed the drilling-induced mechanical damage on the workpiece by measuring the surface topography of drilled holes using Alicona InfiniteFocus Real3D G4 three-dimension optical microscope. Between 10 and 13 holes per condition were drilled in order to reach a steady state temperature [21, 22]. This investigation considered inspection of the last drilled hole in each condition. Table 1 indicates the cutting conditions considered in this study.

Table 1. Drilling conditions utilised in this study for each considered CFRP system (MTM44-1 CF0300, MTM44-1 CF2216 and MTM28B CF0300).

Spindle speed [rpm]	Cutting speed [m/min]	Feed rate [mm/rev]	Penetration rate [mm/min]
2,500	49.8	0.05	125
5,000	99.6		250
7,500	149.4		375
10,000	199.2		500

The surface analysis considered three different locations on each scanned specimen profile: hole entry, middle and hole exit. The size of the scan box was 1,250x200µm, resulting in an actual size of approximately 1,250x220µm after surface area calibration. Figure 1 illustrates an example of a corrected scanned area.

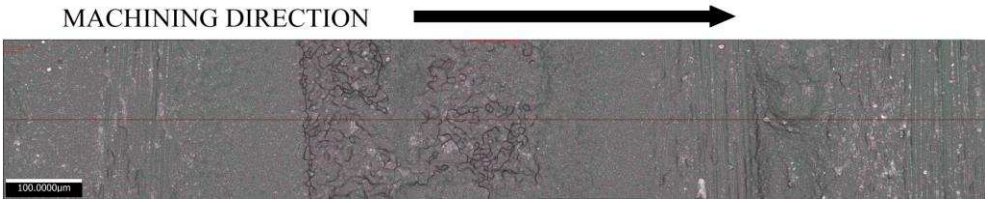

Figure 1. Corrected scanned area of a drilled hole surface. The image allows distinguishing layers having different fibre orientations.

Since FRP composites are heterogeneous, anisotropic, multi-phase materials; statistical study (surface topography analysis) of the drilled profile is more adequate than conventional roughness analysis (profile data along a line). Hence, surface average height (S_a), maximum peak height (S_p) and maximum valley depth (S_v) of the scanned areas compared the surface topography of drilled profiles at different cutting speeds.

2.4 Thermal damage around the hole edge in the drilling of CFRP composites

The objective of this part of the investigation was to assess the drilling-induced thermal damage (ageing), by comparing the bulk mechanical properties of the resin phase of the composite around the

hole exit, where the drilling temperatures reached the local maximum value [22], compared to those of the non-aged resin.

Bulk resin properties (hardness, reduced elastic modulus) were measured applying the nanoindentation technique. The nanoindentation device used was a Veeco Digital Instruments Dimension 3100 scanning probe microscope (SPM) and a Hysitron TS-70 TriboScope fitted with a Cube-Corner diamond tip. Further details about this tip geometry, the device operation procedures and the equations necessary to calculate the tested material hardness, stiffness, reduced modulus of elasticity and modulus of elasticity is available in the literature [23, 25]. Selected specimens were mounted using cold-mounting thermosetting resin and prepared using a Buheler EcoMet 250 grinding-polishing machine.

The grinding stage utilised P400, P800 and P1200 grit size silicon carbide discs, whereas the polishing utilised 6µm, 3µm, 1µm and 0.25µm diamond suspensions. Since the heat generated in the drilling of composites was localised in a small area around the borehole (HAZ) [22], this study measured the bulk resin properties in resin pockets from the hole edge up to 1 mm away, as represented in Figure 2.

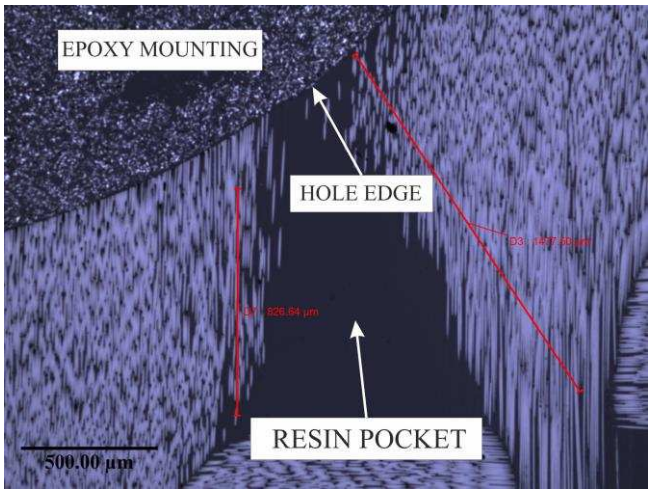

Figure 2. Micrograph showing an example of resin pocket around the hole edge. D3 (1,477.50 µm) and D7 (826.64 µm) indicate the magnitude of the pocket. This image obtained using Nikon Eclipse LV150 optical microscope.

In order to provide more statistical significance to the changes occurring in the very vicinity of the borehole, three consecutive 20x5 indentation arrays covered approximately the initial 60µm distance. Five 5x5 indentation arrays were produced to measure the resin properties at 100µm, 250µm, 500µm, 750µm and 1,000µm respectively.

3 RESULTS AND DISCUSSION

3.1 Mechanical damage around the hole edge in the drilling of CFRP composites

Figure 3 illustrates the values of surface average height (S_a), maximum peak height (S_p) and maximum valley depth (S_v) for the drilled CFRP composites profiles at selected cutting speeds. Results show low surface average height values (10-20 µm) through the inspected hole (Figures 3a, d and g) for all the considered CFRP systems and cutting speeds. However, values of maximum peak height and valley depth indicate dissimilar trends. For MTM44-1 CF2216 composite, Sp and Sv values are consistently low and comparable to those of surface average height (Sa).

On the other hand, composites having HS reinforcement (CF0300) exhibited Sp and Sv values higher and more deviated from their respective values of Sa, especially in the system containing high T_g resin (MTM44-1), at the hole entry and hole exit (Figures 3(b, c), 3(h) and 3(i)).

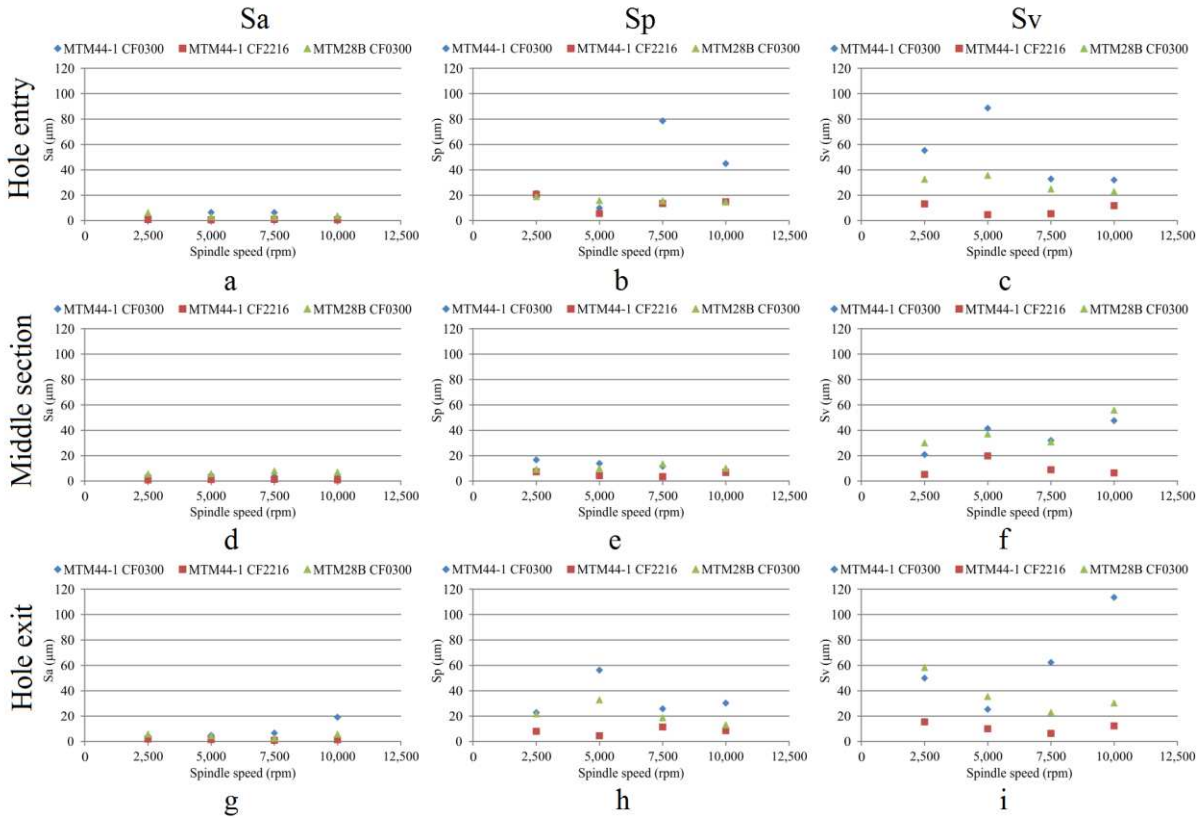

Figure 3. Surface analysis values of the scanned drilled profiles. Top, middle and bottom rows show hole entry, middle section and hole exit values respectively, while left, middle and right columns show surface average height (Sa), maximum peak height (Sp) and maximum valley depth (Sv) measurements respectively.

A possible explanation for these trends is related to the stability of the machining at different drilling stages. At the hole entry, the tool is not fully engaged in the material yet, whereas at the hole exit the tool is no longer backed by the workpiece and the developed temperatures are maximum [22]. Hence, these regions would yield a less stable drilling operation, and less uniform drilled surfaces compared to the middle section. In order to understand the values of Sa, Sp and Sv in this investigation, it is necessary to analyse the 3D surface topography and SEM scans obtained, as depicted in Figure 4.

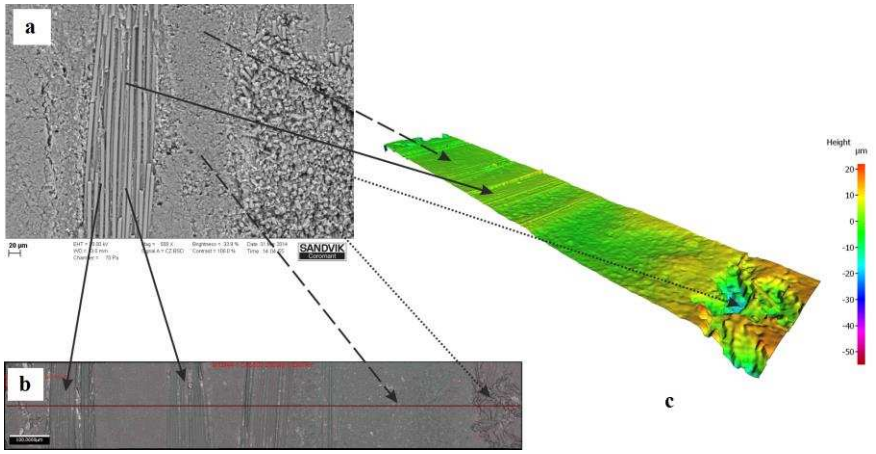

Figure 4. Visual description of the surface topography features in a) SEM, b) 2D corrected surface, and c) 3D surface scans. Continuous, dashed and dotted lines point to areas having approximately 90˚, 0˚ and ±45˚ fibres respectively.

Figure 4(c) shows that maximum heights correspond to areas having 90˚ and ±45˚ fibre orientations. These regions show significant out-of-plane fibres and fibre pull-out, hence Sp values would correspond to these types of defects (splintering and irregularly cut fibres). On the other hand, regions showing negative height values correspond to ±45˚ fibre regions. According to the scans, these regions would develop unclean fibre cutting compared to 0˚ and 90˚ regions, thus removing significant volumes of fibre with resin attached, and creating this type of crater defects.

The increased degree of crystallinity, preferential orientation and lower failure strain of high modulus fibres compared to high strength reinforcement [26-28] promote cleaner fibre cutting, hence explaining the lower values of Sp and Sv. Moreover, the measured depths of the crater-type defects (associated to Sv parameter) are high enough (reaching values around 60 µm in the stable region and 120 µm in the unstable region) to act as fatigue crack initiators and to promote delamination, thus compromising the lifespan of the part and the safety of the structure.

According to the results obtained in this part of the study, workpiece properties, especially the type of fibres, and the orientation of the reinforcement respect to the machining direction showed significant impact on the induced machining damage. Surface average values (Sa) measured on machined surfaces of FRP composites are not representative of their actual damage. Maximum peak (Sp) and depth valley (Sv) parameters provide more valuable information regarding the defects developed (fibre pull-out, splintering and craters) in the machining of FRP composites. Accurate assessment of the damaged surface in the machining of FRP composites requires associating Sp and Sv parameters to the stacking sequence and the machining direction.

3.2 Thermal damage around the hole edge in the drilling of CFRP composites

Figure 5 presents the average values of elastic modulus (E) and hardness (H) calculated from the nanoindentations.

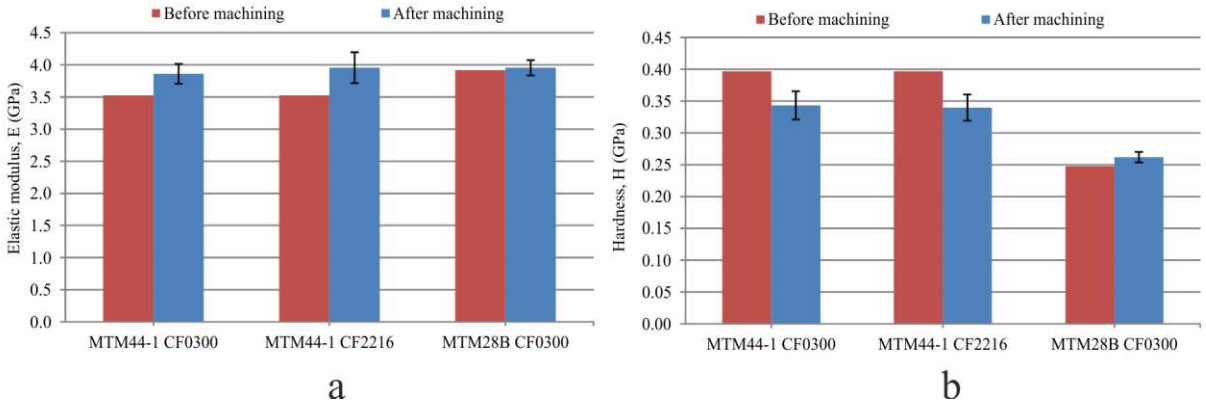

Figure 5. Average values of elastic modulus and hardness of the resin phase around the hole after drilling three CFRP systems at different cutting speeds (blue) and bulk values before drilling (red). These values are also representative of those obtained at all the cutting speeds.

Values of the elastic modulus increased for all the studied systems (Figure 5a), with the difference being greater for the system with highly cross-linked resin (MTM44-1) compared to the system with lower cross-linking density (MTM28B) [21-23]. However, the hardness values (Figure 5b) show a dissimilar behaviour. Composites with MTM44-1 resin exhibited a decrease in hardness, whereas the system with MTM28B showed a slight increase in hardness values. These results indicate a characteristic thermal ageing at different stages of the machining process.

Temperatures developed in the drilling process for the studied systems were higher than their respective T_g in all the cases. Systems having MTM44-1 resin developed temperatures in the workpiece between 205˚C and 250˚C, depending on the type of reinforcement and the cutting speed, whereas MTM28B CF0300 system developed temperatures around 135˚C [21, 22]. These

temperatures were well above (between 25˚C and 70˚C) the curing temperature specified by the manufacturer for MTM44-1-based systems, whereas the MTM28B-based system developed temperatures in the curing temperature range. Therefore, MTM28B-based system would experience a residual cross-linking, followed with an increase in the elastic modulus and hardness, while MTM44-1-based systems would exhibit further ageing, and a decrease in the mechanical properties.

Localised post cross-linking of the resin during the drilling in the regions close to the hole edge would help to explain the increased elastic modulus in MTM44-1 resins.

Another reason that would explain this behaviour and also the elevated values of elastic modulus of MTM28B resin compared to MTM44-1 systems, both before and after drilling, is related to the viscoelastic nature of the epoxies, their respective molecular structures and some limitations of the nanoindentation technique to study polymers. Figure 6 illustrates the morphologies of MTM44-1 and MTM28B resins.

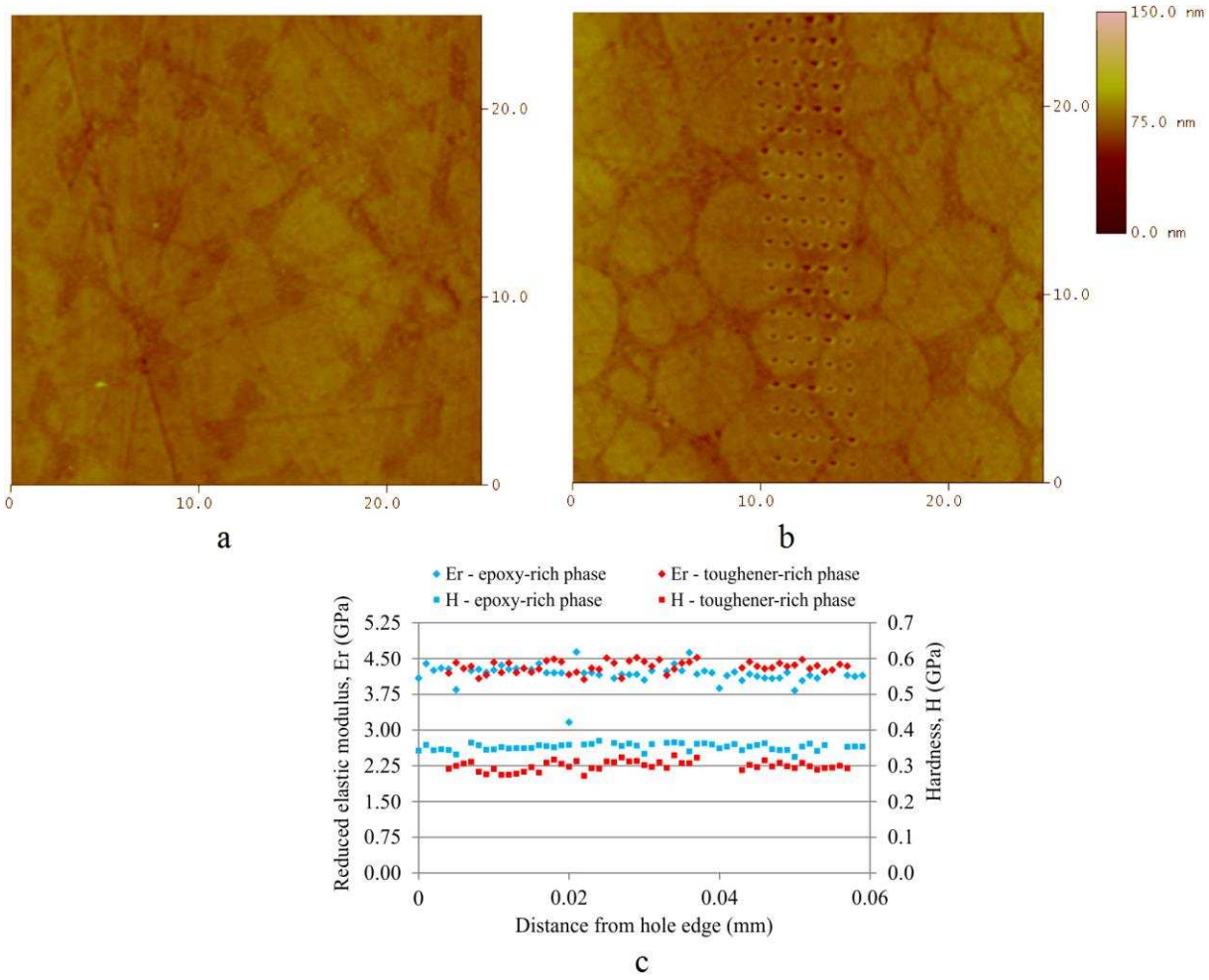

Figure 6. AFM images showing the phase distribution and morphology of a) MTM28B, b) MTM44-1 resins and (c) the hardness and reduced elastic modulus corresponding to the phases in MTM44-1 resin.

The AFM micrographs depicted in Figure 6 revealed highly toughened, two-phase morphologies of the studied resins, however they presented distinct structures. MTM28B resin showed a more uniform phase distribution having a lobe-like toughener-rich phase inside a dominant epoxy-rich phase (Figure 6a). On the other hand, MTM44-1 presented total phase separation where the epoxy-rich phase acquired a globular structure surrounded by a reticulated toughener-rich phase (Figure 6b). Both phases also exhibited differences on their mechanical properties, being more clear for the hardness than for the reduced elastic modulus values (Figure 6c). The epoxy-rich phase yielded consistently

values of hardness above those of the toughener-rich phase; however the difference is not as evident for the reduced elastic modulus, which presented similar values in both phases. In addition to this, the epoxy-rich phase yielded more consistent values of both properties, while the values corresponding to the toughener-rich phase exhibited more fluctuation.

This can be explained because of the yield or relaxation process (related to the partially viscous behaviour of polymers), which is more pronounced in polymers and phases presenting lower degree of cross-linking [3, 4], and the way the reduced elastic modulus is calculated from the nanoindentations [25]. In the nanoindentation of polymers, after the loading stage (or the load hold stage if set), the polymer relaxation process produces the yield flow, therefore varying the maximum indentation depth (h) and load (P). This forms a meniscus (or nose) at the beginning of the unloading stage, more or less pronounced depending on the material and the indentation set-up, which impedes a proper fitting of the tangent at the beginning of the unloading curve. This tangent is used to calculate the stiffness (S) of the material (S=dP/dh), which is then used to obtain the reduced elastic modulus. Hence, the non-proper fitting of the tangent to the unload curve caused by the material flow can lead to anomalous measurements of the reduced elastic modulus.

4 CONCLUSIONS

This investigation assessed the thermal and mechanical damage induced in the drilling of three considered CFRP composites using a range of cutting speeds (50-200m/min), by applying nanomechanical and 3D surface measurement techniques. Based on the experimental results obtained in this work and their analysis, the following conclusions can be drawn:

- The workpiece properties, especially the reinforcement and its relative orientation in respect to the machining direction, have significant impact on the induced mechanical damage and the type of defects. High modulus-reinforced (CF2216) composites yield lower level and smaller defects than those reinforced with high strength fibres (CF0300), which is related to the dissimilar fracture behaviour provided by their distinct crystalline structures and orientations.
- Parameters showing average surface measurements, such as surface average height (Sa), are not representative of the actual damage in the machining of FRP composites. Other parameters indicating the maximum peak heights of valley depths provide a better description and can be related to specific defects, such as splintering, fibre pull-out, delamination and crater formation.
- The size of the crater-type defects measured was high enough (up to 60-120 µm) to initiate and promote fatigue cracks, which would compromise the lifespan and safety of the structure.
- The type of resin and the temperatures developed in the drilling process have an important effect on the induced thermal damage. Different ageing stages (residual cross-linking and further thermal damage) develop depending on the cross-linking degree of the resin, its curing temperature and the ageing temperature.
- Dissimilar ageing behaviour of the phases of the polymer could affect the overall ageing behaviour of the polymer, depending on the nature of the phases, the phase distribution and toughening degree.
- The nanoindentation technique showed to be a valid method to assess the thermal damage in the vicinity of the machined area by measuring the hardness and reduced elastic modulus on the resin phase. Proper measurement and comparison of the reduced elastic modulus requires an ad-hoc setup in order to minimise the effect of the viscous behaviour of the polymer on the measurement.
- Cutting speed did not show a significant impact on the induced thermomechanical damage in the considered range. However, a specific study on the impact of cutting speed on the forces developed in the drilling of CFRP composites will be conducted and related to this investigation.

ACKNOWLEDGEMENTS

This work was co-funded through the EPSRC Industrial Doctorate Centre in Machining Science (EP/I01800X/1) and by Sandvik Coromant. The authors would like to thank Mrs. Dawn Bussey (Department of Materials Science and Engineering, The University of Sheffield) for her assistance to

access and operate the nanomechanical instruments.

REFERENCES

[1] A.J. Timmis, A. Hodzic, L. Koh, M. Bonner, C. Soutis, A.W. Schäfer, L. Dray, Environmental impact assessment of aviation emission reduction through the implementation of composite materials, International Journal of Life Cycle Assessment, **20**, 2014, pp. 233-243.

[2] A.J. Timmis, A. Hodzic, L. Koh, M. Bonner, A.W. Schäfer, L. Dray, Lifecycle assessment of CFRP aircraft fuselage, Proceedings of the 16th European Conference on Composite Materials ECCM16, Seville, Spain, 22-26 June, 2014.

[3] A.J. Lesser, E. Crawford, The role of network architecture on the glass transition temperature of epoxy resins, Journal of Applied Polymer Science, **66**, 1997, pp. 387-395.

[4] E. Crawford, A.J. Lesser, The effect of network architecture on the thermal and mechanical behavior of epoxy resins, Journal of Polymer Science Part B: Polymer Physics, **36**, 1998, pp. 1371-1382.

[5] T.H. Yoon, J.E. McGrath, Curing and toughening of a styrene-modified epoxy resin, Journal of Applied Polymer Science, **80**, 2001, pp. 1504-1513.

[6] J. López, M. Rico, C. Ramírez, B. Montero, Epoxy resin modified with a thermoplastic, Influence of modifier and reaction temperature on the phase separation, Journal of Thermal Analysis and Calorimetry, **99**, 2010, pp. 75-81.

[7] G. Ahmetli, H. Deveci, U. Soydal, S.P. Gurler, A. Altun, Epoxy resin/polymer blends: Improvement of thermal and mechanical properties, Journal of Applied Polymer Science, **125**, 2012, pp. 38-45.

[8] S.T. Kim, J.K. Kim, C.R. Choe, S.I. Hong, Multi-phase toughened epoxy with poly(ether sulphone) and carboxyl-terminated butadiene-acrylonitrile rubber, Journal of Materials Science, **31**, 1996, pp. 3523-3533.

[9] W. Gan, Y. Yu, M. Wang, Q. Tao, S. Li, Viscoelastic effects on the phase separation in thermoplastics-modified epoxy resin, Macromolecules, **36**, 2003, pp. 7746-7751.

[10] B. Russell, R. Chartoff, The influence of cure conditions on the morphology and phase distribution in a rubber-modified epoxy resin using scanning electron microscopy and atomic force microscopy, Polymer, **46**, 2005, pp. 785-798.

[11] J. Zhang, Q. Guo, B. Fox, Structural and material properties of a rapidly cured Thermoplastic-toughened epoxy system, Journal of Applied Polymer Science, **113**, 2009, pp. 485-491.

[12] P. Jyotishkumar, C. Özdilek, P. Moldenaers, C. Sinturel, A. Janke, J. Pionteck, S. Thomas, Dynamics of phase separation in poly(acrylonitrile-butadiene-styrene)- modified epoxy/DDS system: Kinetics and viscoelastic effects, Journal of Physical Chemistry B, **114**, 2010, pp. 13271-13281.

[13] J. Moosburger-Will, J. Jäger, S. Horn, C. Wellhausen, Investigation of phase morphology of polyetherimide-toughened epoxy resin by scanning probe microscopy, Polymer Testing, **31**, 2012, pp. 1008-1018.

[14] M. Rico, J. López, B. Montero, R. Bellas, Phase separation and morphology development in a thermoplastic-modified toughened epoxy, European Polymer Journal, **48**, 2012, pp. 1660-1673.

[15] V.S. Mathew, S.C. George, J. Parameswaranpillai, S. Thomas, Epoxidized natural rubber/epoxy blends: Phase morphology and thermomechanical properties, Journal of Applied Polymer Science, **131**, 2014, pp.

[16] H. Tanaka, T. Araki, Phase inversion during viscoelastic phase separation: Roles of bulk and shear relaxation moduli, Physical Review Letters, **78**, 1997, pp. 4966-4969.

[17] H. Tanaka, Viscoelastic phase separation, Journal of Physics Condensed Matter, **12**, 2000, pp. 207-264.

[18] S.R. Jong, T.L. Yu, Physical aging of poly (ether sulfone)-modified epoxy resin, Journal of Polymer Science, Part B: Polymer Physics, **35**, 1997, pp. 69-83.

[19] A. Lee, G.B. McKenna, Anomalous aging in two-phase systems: Creep and stress relaxation differences in rubber-toughened epoxies, Journal of Polymer Science, Part B: Polymer Physics, **35**, 1997, pp. 1167-1174.

[20] T. Leon Yu, Y.S. Chen, Physical aging of epoxy resin blended with poly(ether sulfone): Effect of poly(ether sulfone) molecular weight, Journal of Polymer Research, **7**, 2000, pp. 257-266.

[21] J.L. Merino-Pérez, E. Merson, S. Ayvar-Soberanis, A. Hodzic, The applicability of Taylor's model to the drilling of CFRP using uncoated WC-Co tools: The influence of cutting speed on tool wear, International Journal of Machining and Machinability of Materials, **16**, 2014, pp. 95-112.

[22] J.L. Merino-Pérez, R. Royer, S. Ayvar-Soberanis, E. Merson, A. Hodzic, On the temperatures developed in CFRP drilling using uncoated WC-Co tools Part I: Workpiece constituents, cutting speed and heat dissipation, Composite Structures, **123**, 2015, pp. 161-168.

[23] J.L. Merino-Pérez, A. Hodzic, E. Merson, S. Ayvar-Soberanis, On the temperatures developed in CFRP drilling using uncoated WC-Co tools Part II: Nanomechanical study of thermally aged CFRP composites, Composite Structures, **123**, 2015, pp. 30-34.

[24] J.L. Merino-Pérez, S. Ayvar-Soberanis, E. Merson, A. Hodzic, The influence of heat during short ageing periods on the mechanical properties of CFRP composites, Proceedings of the 16th European Conference on Composite Materials ECCM16, Seville, Spain, 22-26 June, 2014.

[25] W.C. Oliver, G.M. Pharr, Improved technique for determining hardness and elastic modulus using load and displacement sensing indentation experiments, Journal of Materials Research, **7**, 1992, pp. 1564-1580.

[26] R.H. Knibbs, J.B. Morris, The effects of fibre orientation on the physical properties of composites, Composites, **5**, 1974, pp. 209-218.

[27] N.C. Gallego, D.D. Edie, Structure-property relationships for high thermal conductivity carbon fibers, Composites - Part A: Applied Science and Manufacturing, **32**, 2001, pp. 1031-1038.

[28] G. Yuan, X. Li, Z. Dong, A. Westwood, B. Rand, Z. Cui, Y. Cong, J. Zhang, Y. Li, Z. Zhang, J. Wang, The structure and properties of ribbon-shaped carbon fibers with high orientation, Carbon, **68**, 2014, pp. 426-439.